Simultaneous PET-MR-EEG: Technology, Challenges and Application in Clinical Neuroscience

I. Neuner, R. Rajkumar, C. Régio Brambilla, S. Ramkiran, A. Ruch, L. Orth, E. Farrher, J. Mauler, C. Wyss, E. Rota Kops, J. Scheins, L. Tellmann, M. Lang, J. Ermert, J. Dammers, B. Neumaier, C. Lerche, *Member, IEEE*, K. Heekeren, W. Kawohl, K.-J. Langen, H. Herzog, *Senior Member, IEEE*, and N. J. Shah

***Abstract*—Due to technological developments in positron emission tomography (PET) detectors and PET-MR integration, the simultaneous measurement of PET-MR-EEG has become feasible, offering the possibility of exploring the complementary information provided by each modality. Studies have already shown the benefits of simultaneous measurement using PET-MR, however, such achievements come with different technical and practical challenges. In this context, we aim to give an overview of the technical challenges involved in integrating electroencephalography with hybrid PET-MR scanners and demonstrate possible solutions. When acquiring simultaneous data from multiple modalities, the data acquisition protocol should be optimized in order to utilize time and complementary information most effectively. Thus, practical considerations with regard to protocol optimization are also discussed, alongside relevant examples. In addition to simultaneous data acquisition, another major challenge is the integration of the multimodal data, which is also addressed. Finally, a clinical application with a strong focus on neuro-psychiatry is shown. This clinical application is discussed with relevant examples from an ongoing clinical study. Finally, the possibility of utilizing the PET-MR-EEG data in search for new biomarkers for individualized medicine in clinical neuroscience is briefly explored.**

***Index Terms*—Biomarkers, electroencephalography (EEG), magnetic resonance imaging (MRI), positron emission tomography (PET).**

Manuscript received September 11, 2018; accepted November 7, 2018. Date of publication December 20, 2018; date of current version May 2, 2019. *(I. Neuner and R. Rajkumar contributed equally to this work.) (Corresponding author: I. Neuner.)*

I. Neuner and R. Rajkumar are with the Institute of Neuroscience and Medicine 4, Forschungszentrum Jülich, 52425 Jülich, Germany, also with the Department of Psychiatry, Psychotherapy and Psychosomatics, RWTH Aachen University, 52062 Aachen, Germany, and also with JARA—BRAIN—Translational Medicine, 52056 Aachen, Germany (e-mail: i.neuner@fz-juelich.de).

C. Régio Brambilla, S. Ramkiran, A. Ruch, and L. Orth are with the Institute of Neuroscience and Medicine 4, Forschungszentrum Jülich, 52425 Jülich, Germany, and also with the Department of Psychiatry, Psychotherapy and Psychosomatics, RWTH Aachen University, 52062 Aachen, Germany.

E. Farrher, J. Mauler, E. Rota Kops, J. Scheins, L. Tellmann, J. Dammers, C. Lerche, and H. Herzog are with the Institute of Neuroscience and Medicine 4, Forschungszentrum Jülich, 52425 Jülich, Germany.

C. Wyss, K. Heekeren, and W. Kawohl are with the Department of Psychiatry, Psychotherapy and Psychosomatics, University Hospital of Psychiatry, 8032 Zürich, Switzerland.

M. Lang, B. Neumaier, and J. Ermert are with the Institute of Neuroscience and Medicine 5, Forschungszentrum Jülich, 52425 Jülich, Germany.

K.-J. Langen is with the Institute of Neuroscience and Medicine 4, Forschungszentrum Jülich, 52425 Jülich, Germany, and also with the Department of Nuclear Medicine, RWTH Aachen University, 52062 Aachen, Germany.

N. J. Shah is with the Institute of Neuroscience and Medicine 4, Forschungszentrum Jülich, 52425 Jülich, Germany, also with JARA—BRAIN—Translational Medicine, Aachen, Germany, also with the Institute of Neuroscience and Medicine 11, Forschungszentrum Jülich, 52425 Jülich, Germany, and also with the Department of Neurology, RWTH Aachen University, 52062 Aachen, Germany.

Color versions of one or more of the figures in this paper are available online at http://ieeexplore.ieee.org.

Digital Object Identifier 10.1109/TRPMS.2018.2886525

I. Introduction

NEW DEVELOPMENTS in all fields of medical imaging technology have paved the way for the simultaneous acquisition of magnetic resonance imaging (MRI) and positron emission tomography (PET) [1]–[3]. The key element, and main advantage of this approach, is that structural and functional (via MRI) and metabolic (via PET) signatures can be assessed simultaneously under the same physiological and psychological conditions. As neuronal networks function and regroup in a time frame of milliseconds, the high temporal information provided by electroencephalography (EEG) is also highly desirable. In this paper, we highlight the technical challenges arising from the combination of the three very distinct imaging techniques. Examples of hybrid MR-PET protocols will be given alongside the initial results of clinical studies which aim to search for biomarkers to enable individualized medicine in clinical neuroscience.

II. Integration of EEG Into PET-MR

In general, when integrating multiple modalities as a single unit, the mutual interferences between the modalities should be taken into account. The mutual interferences caused by each modality on the other modalities should either be avoidable (via using mutually compatible components) or corrigible (via signal/image processing techniques) with minimum or no loss of the desired data. The mutual interferences between PET and MR components in hybrid PET-MR scanners have been

well studied and reported [4]–[7]. Hence, in this section, only a brief overview of the technical challenges and possible solutions for integrating EEG in to hybrid PET-MR scanners will be given.

A number of MR-compatible EEG systems are commercially available for use inside MR scanners. The main components of an MR-compatible EEG system include an MR-compatible amplifier, a power source, an electrode cap with electrodes (EEG cap), and cables for connecting the amplifier with the EEG cap. All of these components are usually placed inside the bore of the MR scanner for the simultaneous acquisition of MR and EEG data. In addition to these components, a synchronization unit (to synchronies the clock of the EEG amplifier with the clock of the MRI scanner's gradient switching system) and an EEG recording unit (a computer system with software for recording EEG signals) are located inside the MR control room. Such commercially available MR-compatible EEG systems can only be used in hybrid MR-PET scanners if the components used in the EEG cap (which are in direct contact with the subject's head) cause very minimal, or no attenuation, to the 511 keV photons emitted by the PET radiotracer; or if their attenuation can be corrected. In a recent study using a 3T MR-BrainPET scanner (Siemens, Erlangen, Germany [8], [9]), we have shown that the attenuation effect of an EEG cap on PET images is inconsequential, provided that the materials used in the electrode housing and fabric have very low attenuation coefficient and that the metallic electrodes and chip resistors used in the EEG cap are extremely thin. In addition to this, care should be taken to avoid the presence of the ribbon / bundle cable (used to connect the EEG cap and amplifier) inside the field of view (FOV) of the PET detectors (Fig. 1). Furthermore, in order to gain a better signal-to-noise ratio (SNR) for EEG data, a short bundle cable is recommended [10].

Even though the EEG system is MR compatible, due to high radio frequency (RF) power dissemination, a small number of MR sequences may cause a greater heating effect on the metal electrodes in the EEG cap [11]. Hence, only the MR sequences which are EEG friendly, as informed by the EEG system vendor, should be performed during simultaneous PET-MR-EEG data acquisition.

In addition to the compatibility of the components used in the system, artifacts in the EEG data, due to hybrid PET-MR scanner, should also be considered. Such artifacts can be broadly classified into the following groups: imaging related, motion related, and cardiac-related artifacts. A brief summary of each artifact and possible solutions for correction are discussed below.

A. MR Imaging-Related Artifacts

The switching of magnetic gradients is necessary for MRI data acquisition. Two types of distinguishable imaging artifacts are the gradient artifact (GA), which causes a massive distortion of the EEG signal, and RF artifacts. The GA distorts the EEG spectrum over a broad frequency range and fluctuates over time with respect to the slice acquisition time. It generates

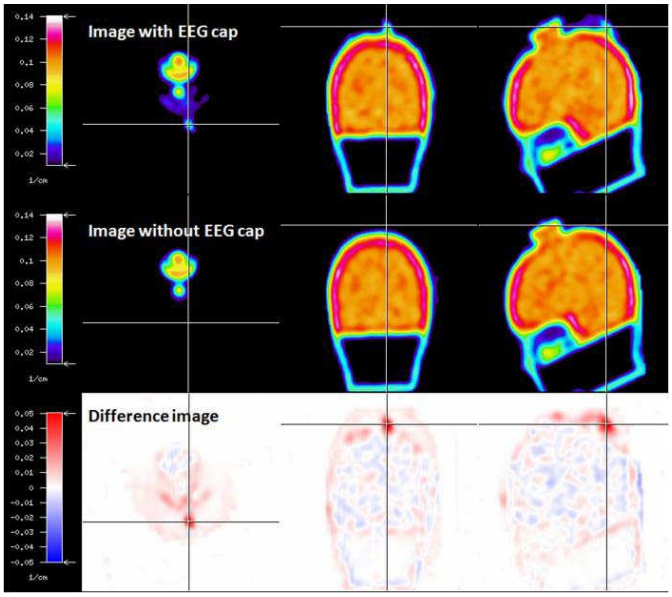

Fig. 1. Attenuation maps of the Iida brain phantom [10] with an EEG cap (upper row) and without an EEG cap (middle row); difference image (bottom row). The images were obtained by performing a 60 min transmission scan using an ECAT HR+ scanner (CTI/Siemens, Knoxville, TN, USA) on the Iida brain phantom. The images on the upper row were obtained by placing a 32 channel BrainCap MR EEG cap (EASYCAP GmbH, Herrsching, Germany) on the Iida brain phantom, and the middle row images were obtained after removing the BrainCap MR EEG cap. The image on the bottom row shows the difference between the images with and without the EEG cap. The position of the ribbon cable, shown by the cross lines in the difference image, shows a maximum attenuation of about 0.05/cm. Therefore, it is recommended that the ribbon cables/bundle cable of the EEG cap should be brought outside the FOV of the PET detectors.

fast transients with large amplitudes, which are comparatively higher than EEG signals. Thus, the recorded signals contain linearly mixed GA and EEG signals [Fig. 2(a)]. This linear mixing makes the GA more disposed to removal using signal processing methods. Average artifact subtraction (AAS) [12] is an effective method to remove the GA from EEG signals which have been recorded simultaneously with functional MRI (fMRI). AAS includes two steps: first, an average of the GA is calculated using a fixed number of epochs and subtracted from the EEG, and second, any residual GA is reduced from the EEG by using adaptive noise cancelling [Fig. 2(b)]. Unlike GA, RF artifacts occur at a very high frequency range, which is usually filtered out by the low pass filter in the EEG amplifier.

B. Motion Related Artifacts

The movement of conductive materials, such as EEG electrodes and cables, in the static magnetic field of the MR scanner induces voltages and/or currents. Thus, even a minute movement of the subject's head in the scanner will contaminate the EEG signal. In addition, at least two types of vibration induced motion can contaminate the EEG signal: the vibration due to the scanner cryogen pump and the vibration induced by the gradient switching itself. Both of these vibrations can cause motion of the subject and/or of the EEG system. In addition to vibration induced motion, endogenous, and inevitable

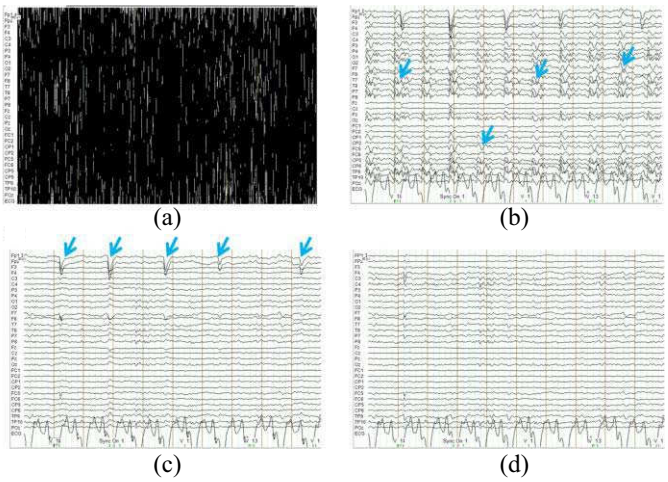

Fig. 2. Section of simultaneously recorded EEG channels showing different artifacts and cleaned EEG signal. EEG channels shown in all four figures correspond to the same section. (a) EEG channels showing the GA riding on top of the EEG signal. (b) EEG signal after GA removal using the AAS algorithm. Additional filtering was performed using Butterworth zero phase filter with lower cut-off frequency of 0.16 Hz and higher cut-off frequency of 8 Hz for the ECG channel and 16 Hz for other EEG channels. Some of the cardiac related artifacts, which are visible after GA correction, are indicated by blue arrows. (c) EEG signal after cardiac related artifacts were removed using the AAS algorithm. The ocular artifacts, which are more prominent in the frontal channels, are indicated by blue arrows. (d) EEG signal after ocular correction performed using an algorithm proposed by Gratton *et al.* [15] (1983).

motion related artifacts are induced by the subject's breathing and cardiac cycle. Another seemingly unavoidable artifact is the ocular artifact. This occurs as a result of the movement of the eyeballs or eye blinking [Fig. 2(c)]. A number of methods have been proposed to correct these types of artifacts [13]–[15] [Fig. 2(d)].

The vibration induced artifacts due to the cryogen pumps are scanner specific. These artifacts affect the EEG frequency spectrum starting from 20 Hz for the 3T Tim Trio (Siemens, Erlangen, Germany) scanner and 30 Hz for the Verio (Siemens, Erlangen, Germany) scanner [16]. Vibration induced artifacts due to the cryogen pump can be avoided by switching off the cryogen pump system during the simultaneous measurement, if the MR system allows this. If this is not possible, such artifacts can be corrected using a template subtraction method [17].

Motion related artifacts are unavoidable. Simple head motions such as nodding and shaking greatly affect the low frequency spectrum (less than 10 Hz) [18] of the EEG signals. A number of techniques have been proposed for motion correction [19]–[21], but none offer perfect correction of motion related artifacts [22]. Considering the difficulties associated with the correction of motion related artifacts, many studies simply remove the period of EEG data during motion via visual inspection [23], [24]. However, to some extent, motion can be controlled by rigidly fixing the subject's head. Also vibrations resulting from gradient switching can be minimized by placing sand bags over the cables and amplifier.

C. Cardiac-Related Artifacts

Unlike other artifacts, the ballistocardiogram (BCG) artifact is always present during the entire acquisition. BCG contributes to the low frequency portion of the EEG signal (<15 Hz). The exact origin of the BCG is not known yet, although it seems to be due to the pulsatile flow of blood associated with the cardiac cycle.

In simultaneously recorded EEG signals, BCG artifacts are clearly visible in all channels after removing the GA [Fig. 2(b)]. A delay between the R peak of the ECG and the peak amplitude of the BCG artifact in EEG traces is identifiable. AAS [24] is a method widely used to remove BCG artifacts. In this approach, the onset of the cardiac cycle is first estimated, and then a BCG artifact template is defined by a moving average procedure for each EEG channel separately. Later, this template is subtracted from each artifact occurrence [Fig. 2(c)].

Other approaches for the removal of BCG artifacts have also been proposed. For example, the optimal basis set method [25] uses a channel wise temporal principal component analysis to calculate the BCG artifact template. An adaptive Kalmann filter approach has also been proposed [23], although it requires an additional motion sensor signal to be recorded as a reference signal. Independent component analysis (ICA) based methods [26], [27] can also be used to remove BCG artifacts.

III. Simultaneous PET-MR-EEG Data Acquisition Protocol

One of the main challenges in the acquisition of PET data alongside MR and EEG data is the optimization of the PET tracer injection protocol. The tracer may be injected either as a bolus or bolus plus infusion. In either case, the fMRI and EEG data of interest are recorded only after the PET tracer reaches equilibrium in the organ of interest. Either for bolus or for bolus plus infusion protocols, the tracer is usually injected while the subject is lying in the hybrid PET-MR scanner with the EEG cap already in position on their scalp. The tracer is injected via an intravenous line. The PET data acquisition can start before or after the injection of the tracer depending on the experimental protocol. The PET data are continuously acquired in dynamic list mode during the whole experiment. The PET data acquisition in dynamic list mode offers the flexibility of data reconstruction as per the study design. The time until the tracer reaches equilibrium can be utilized effectively by performing scans for obtaining structural MRI, or attenuation maps. To eliminate the need for additional scans to obtain the attenuation map, structural MRI-based attenuation corrections can be performed [28].

In principle, any MRI sequence can be applied along with PET acquisition, however each MRI sequence causes a varying count rate reduction in PET data [5], [29], [30]. The count rate reduction can be corrected by interpolation.

As mentioned above, the PET tracer may be injected either as a bolus or bolus plus infusion. A brief overview of bolus plus infusion protocols with regard to nondisplaceable binding potential (BP_{ND}) calculations is given below.

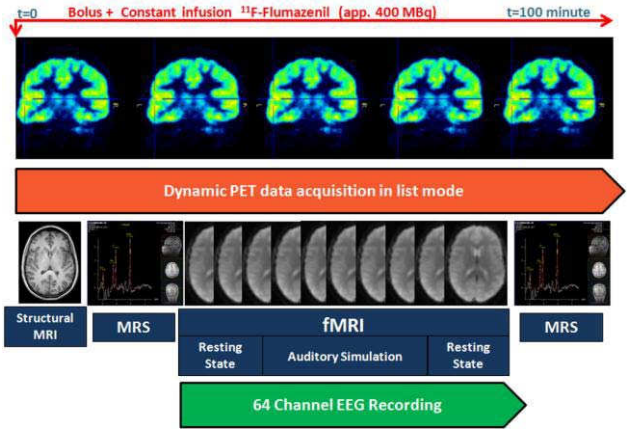

Fig. 3. Simultaneous trimodal data acquisition protocol for [^{11}C] FMZ PET, MR, and EEG.

Bolus plus infusion PET protocol usually aims to measure the BP_{ND} while the tracer reaches equilibrium in the organ of interest. This protocol is normally performed by administering a portion of the prepared tracer as an initial bolus, followed by a constant infusion of the tracer during the entire PET data acquisition. If the bolus and infusion fractions are balanced correctly, the time activity curves (TACs) in the region(s) of interest will reach equilibrium in a minimal amount of time [31]. At the equilibrium condition, the tracer concentrations in plasma, in both free and bound compartments, will remain in constant proportion. The main advantage of the bolus plus infusion protocol is that during the equilibrium condition, the BP_{ND} can be calculated as a simple ratio. The BP_{ND} is calculated as $(C\text{-}C')/C'$, where C denotes the activity concentration in an area of high receptor density and C' denotes the activity concentration in an area of very low receptor density (reference region). The main drawback of the bolus plus infusion protocol is the difficulty associated with infusing the tracer at a constant rate. This may be overcome by infusing the tracer using an MR compatible infusion pump. In addition to this drawback, the optimal bolus to infusion ratio may vary among subjects. This may lead to a delay in reaching the equilibrium condition. As an example of a bolus plus infusion protocol, a pilot trimodal approach, aimed to combine hybrid PET-MR with EEG to investigate the role of the GABAergic system with the loudness dependence of auditory evoked potentials response, is presented here [32] (Fig. 3). In this explorative study, fMRI, [^{11}C] Flumazenil (FMZ) PET, and EEG data were recorded simultaneously in a healthy male subject during acoustic stimulation. An application of such a trimodal approach for a clinical study would be the investigation of medication resistant epilepsy patients who are considered for neurosurgical intervention. The trimodal setup using [^{11}C]FMZ would also allow for the investigation of the GABAergic deafferentation hypothesis in age and Alzheimer's disease related neuronal degeneration [33].

In total, 401 MBq of [^{11}C]FMZ was injected according to the bolus and constant infusion scheme with $k_{\mathrm{Bol}} = 46.22$ min over a period of 100 min. PET data acquisition in list mode started immediately in conjunction with the bolus injection (volunteer lying in the hybrid PET-MR scanner). With this protocol, equilibrium in the TACs was reached after 30–35 min [34]. The PET data were iteratively (3-D OSEM, 32 iterations, and 2 subsets) reconstructed (frame length 30 × 200 s, 256 × 256 × 153 voxels, and 1.25 × 1.25 × 1.25 mm^3), filtered (2.5 mm 3-D Gaussian), and motion corrected. An MR- and template-based attenuation correction was applied [28]. EEG signals were recorded simultaneously with PET and fMRI, using a 64-channel MR compatible EEG system (Brain Products GmbH, Germany).

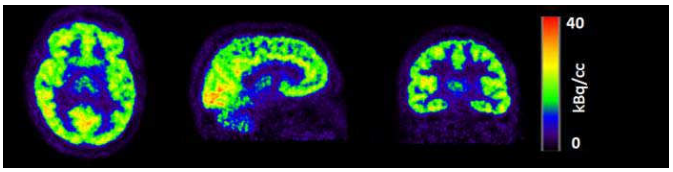

Fig. 4. [^{11}C] FMZ PET image in different orientations of the subject during auditory stimulation. The PET image was obtained by averaging the image frames obtained during first 10 min of auditory stimulation.

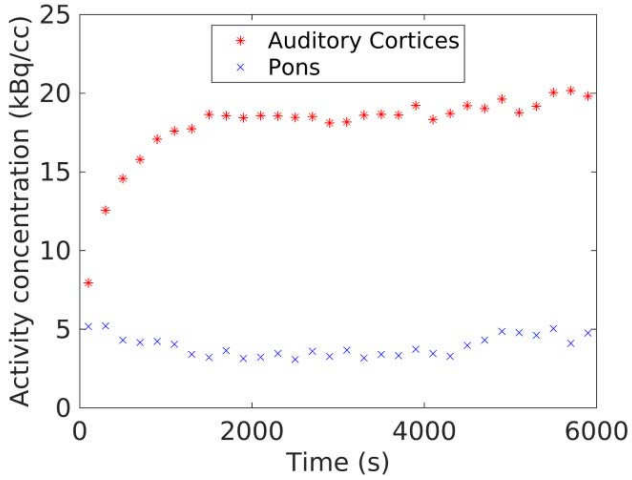

Fig. 5. Graph showing the average activity in the auditory cortices and pons during the entire PET measurement.

PET data analysis was performed using the PMOD software package (Version 3.5, PMOD, Zürich, Switzerland, https://www.pmod.com/web). The [^{11}C]FMZ PET image of the subject averaged across the first 10 min of the auditory stimulation is shown in Fig. 4. The binding potential (BP) of [^{11}C]FMZ was calculated from the auditory cortex in both hemispheres of the brain. The Pons, a region with no measurable specific binding for [^{11}C]FMZ as reported in a previous study [35], was chosen as the reference region. The BP during the time frame of auditory stimulation in the auditory cortices was found to be 4.9 ± 0.3. The activity concentration of [^{11}C]FMZ in the auditory cortices and in the pons is shown in Fig. 5.

The results presented here show that it is possible to record and analyze PET data simultaneously with EEG and fMRI.

IV. Multimodal Data Integration and Analysis Techniques

Multimodal brain imaging provides fingerprints of hemodynamic, metabolic, and electrophysiological activity in the

living human brain in such a way that structural and functional information is recorded in synchrony. Each modality of any hybrid brain-imaging scanner, however, operates at different spatial and temporal scales, thus providing various measures of biophysical quantities at different resolutions and at different SNRs. These multivariate datasets make it possible to uncover spatio-temporal dynamics of the living human brain. However, data analysis remains challenging. Not only does the spatial and temporal resolution of the acquired information differ across modalities, but also the nature of the data. Each modality measures distinct features of the same biological process and/or complementary features from different biological processes.

Typically, data analysis is applied separately for each modality's data, thus ignoring the comprehensive information content of the simultaneously recorded data. Recent endeavors from various neuroimaging groups claim that there is a need for combining and extracting all available information from the multivariate data sets in order to better understand the spatio-temporal dynamics underlying specific brain functions [36]–[38]. One important aspect of such multimodal data analysis would be the maximum utilization of complementary information provided by each modality in to the analysis of another modality. Integrated analysis can be done either to increase the sensitivity and specificity of diagnosis [39] or to better understand the physiological processes [40]. Machine learning methods are also being proposed for multimodal data integration [41]. Such integrated data analysis is broadly classified in to two types: 1) symmetric data fusion and 2) asymmetric data fusion.

A. Symmetric Data Fusion

In this type of data fusion, the complementary information from each modality is considered to be on par and are analyzed jointly. A typical example of this type of data fusion is the utilization of the structural information afforded by MRI and the metabolic information from PET to aid tumor diagnosis [42]. Furthermore, the symmetric data fusion approach may be either data-driven [43] or hypothesis-driven [44].

B. Asymmetric Data Fusion

In this type of data fusion, data from one modality is given higher emphasis than another modality. A typical example would be using a feature obtained from one modality as a predictor for another modality [45].

Even though a large number of algorithms and methods are available for the integration of multimodal data, the choice of method is dependent on the research hypothesis under question.

V. Clinical Applications

Advances in every aspect of multimodal neuroimaging will help to further understanding of the brain's structure and function. In addition, multimodal neuroimaging can be used to identify new biomarkers for neurological and psychiatric disorders [46]. Detailed reviews of potential applications of multimodal neuroimaging have been discussed in [47]–[49]. Furthermore, such multimodal imaging set-ups are essential in pharmacological challenge studies, where sequential measurements would add confounding factors [50].

For the purpose of this paper, an example of multimodal neuroimaging in clinical neuro-psychiatry is discussed below.

Previous studies have shown both structural, as well as functional abnormalities, in various neuro-psychiatric disorders [49]. Accessing the structural, functional, metabolic, and electrophysiological signatures simultaneously will add value in disease diagnosis, treatment planning, and the monitoring of psychiatric disorders [51]. As an example, an overview of the study design, and analysis of simultaneously acquired PET-MR-EEG data in an ongoing study with schizophrenic patients is presented here. The study was designed to explore the feasibility of recording, and also to validate the simultaneous trimodal acquisition protocol on a 3T MR-BrainPET scanner (Siemens, Germany) equipped with a 64-Channel MR compatible EEG system (Brain Products, Germany) [52]. The PET part of the trimodal setup targeted the metabotropic glutamate receptor 5 (mGluR5) using [^{11}C]ABP688 as tracer. mGluR5 is a G-protein–coupled receptor that activates the intracellular secondary system when bound by glutamate. mGluR5 has been an important focus area for research in a variety of disorders, including anxiety [53], [54], depression [53], schizophrenia [55], Parkinson's disease [56], and drug addiction [57]. PET data acquisition in list mode started immediately following an injection of the [^{11}C]ABP688 tracer. MRI (structural and functional) data were simultaneously recorded with the PET acquisition. When the tracer reached a steady-state after 30 min, the EEG data was also recorded. A rest–task–rest fMRI measurement protocol was used. During the resting state (rs) the subject was instructed to close his eyes (eyes closed rs) and during the task, an auditory mismatch negativity paradigm was played. To indicate the feasibility of this approach, only the processing and first pilot results from the PET-MR-EEG data obtained during the first rs measurement are presented here. These data were obtained from a healthy male volunteer (control, age 28) and a schizophrenic patient (age 26). This paper was conducted according to the Declaration of Helsinki and prior, written consent was obtained from both volunteers.

A. PET Data

Both the patient and the volunteer were injected with 572 ± 28 MBq of [^{11}C]ABP688 [58], [59] via bolus injection plus constant infusion, with $k_{\mathrm{Bol}} = 53$ minutes over a period of 65 min [60], [61]. Data were acquired in list mode, then iteratively reconstructed with 3-D OSEM 32 iterations and 2 subsets, 22 frames of 10×60 s; 6×180 s, and 6×300 s, 253 slices, voxel 1.25 mm^3 isotropic. MR-template-based attenuation correction [28], [62] was performed. PET data were corrected for decay, dead time, random, and scatter coincidences. PET images were smoothed with a 3 mm Gaussian kernel and motion corrected, using Pmod software package. The $\mathrm{BP_{ND}}$ was calculated during the equilibrium period [63] (30 min after the tracer injection) from the default

mode network (DMN) regions in the brain. The Cerebellum, which has negligible binding to mGluR5 [59], [63] was chosen as the reference region.

B. fMRI Data

fMRI data analysis was performed using a MATLAB-based toolkit, DPABI [64]. DPABI contains libraries for processing fMRI data that depend on another MATLAB-based software package, Statistical Parametric Mapping 12 (SPM12, Welcome Trust Centre for Neuroimaging). One of the data driven functional connectivity measures, called degree centrality (DC) [65], was computed using rs-fMRI data from both the healthy control and the schizophrenic patient. The DC measure estimates the number of direct functional connections between a given voxel and all the other voxels in the brain. The functional connectivity measure was computed after pre-processing steps, which included corrections for slice timing, motion, and nuisance signal. Temporal filtering was performed between 0.01 and 0.08 Hz. DC values (correlation cut-off - Pearson $r > 0.25$, $p < 0.0001$) were calculated in the subjects' native space and were linearly standardized to Z values. Z standardized connectivity measures were then co-registered to the standard MNI space (voxel size 2 mm3 isotropic).

The DMN functional regions mask was obtained from the 90 fROI atlas [66] by combining dorsal and ventral DMN masks. A whole brain gray matter (GM) mask was made by segmenting the MNI152 brain template using the FSL FEAT [67] software package. The DMN functional mask was corrected for GM using the GM mask created. In-order to quantify the changes in DC measure between the healthy control and the schizophrenic patient, voxel values within the GM corrected DMN functional region were extracted.

A two sample t-test was performed in MATLAB software (Version 8.5, Matworks) to compare DC values between the healthy control and the schizophrenic patient.

C. EEG Data

Functional and effective connectivity can also be assessed through EEG data. One such measure to assess functional connectivity is synchronization likelihood. It is a measure of generalized synchronization between time-series data, and unlike many commonly used measures, it captures both the linear and nonlinear synchronization of signals [68]. Graph theory can be applied to these measures to map the network topological organization of the brain. In healthy individuals, these networks have been shown to be intrinsically organized as small world networks [69].

EEG data were preprocessed using EEGLAB [70] and BrainVision Analyzer (BrainProducts GmbH, Gilching, Germany). The EEG data recorded exactly during first rs measurement were considered in this analysis. GA correction was performed using the EEGLAB FMRIB plug-in [12] and [25]. EEG data were down-sampled to 1024 Hz and exported to the BrainVision Analyzer for semi automated QRS event detection. After QRS detection, the EEG data were imported back to EEGLAB. Cardioballistic correction was performed using the EEGLAB FMRIB plugin. This was followed by band pass filtering (0.5–100 Hz) and by removal of sinusoidal line noise at 50 Hz using an EEGLAB CLeanLine plugin (http://www.nitrc.org/projects/cleanline/). EEG data were referenced using the average reference of all the EEG channels, and ICA decomposition was performed using the extended Infomax algorithm [71]. Artifactual components were removed by visual inspection of spectral information, scalp maps, and time varying activations and parameters computed using SASICA [72]. Components with a peak time locked to the R-peak and with perfectly symmetrical maps were also removed.

The artifact corrected EEG data were then band-pass filtered to the alpha1 frequency band (8–10 Hz), and exported to Brain Vision Analyzer, where source localization was performed using LORETA [73]. Synchronization Likelihood was computed for the source localized EEG data. The connectivity matrices had a threshold at 0.1 (> 0.1 or < -0.1) and graph theory was applied.

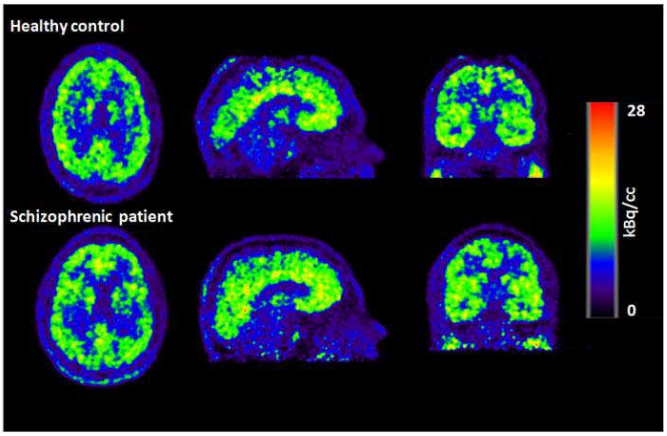

Fig. 6. PET images of the healthy control (top row) and schizophrenic patient (bottom row) acquired during the first rs measurement.

D. Results

The PET, fMRI, and EEG measures were calculated as explained above. The PET images of the control subject and schizophrenic patient during the first rs measurement are shown in Fig. 6. The TACs of the healthy control subject and schizophrenic patient during the whole PET measurement are shown in Fig. 7. The BP_{ND} values calculated in the DMN regions for the healthy control subject and schizophrenic patient are plotted Fig. 8.

The DC values of the control subject and schizophrenic patient calculated during the first rs measurement are shown in Fig. 9. The two sample t-test between the healthy control and the schizophrenic patient show a significant difference ($p < 0.0001$) for fMRI DC values in the DMN region. The voxel value distribution for fMRI DC measure is shown in Fig. 10

A trend of increased synchronization likelihood can be observed in the DMN regions of the schizophrenic patient compared to the healthy control (Fig. 11).

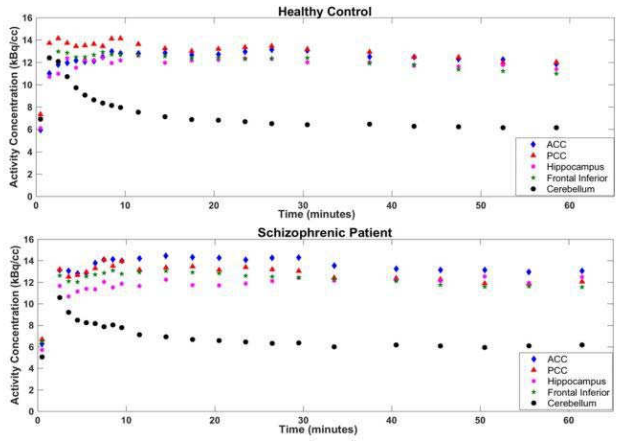

Fig. 7. TACs from (a) healthy volunteer and (b) schizophrenic patient matched for age, smoking status, gender, and education. A steady-state in richest (anterior cingulated cortex, posterior cingulated cortex, hippocampus, frontal inferior), and poorest (cerebellum) receptor density regions is reached 30 min after the bolus injection.

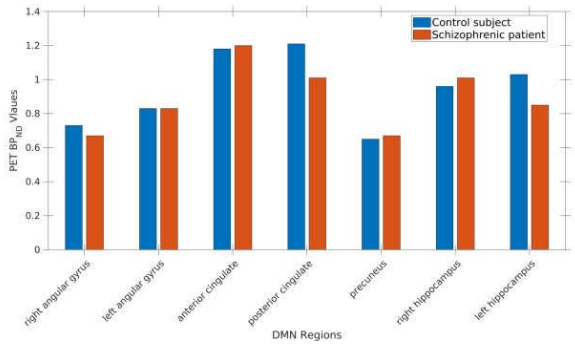

Fig. 8. BPND values of the healthy control and the schizophrenic patient in the DMN regions.

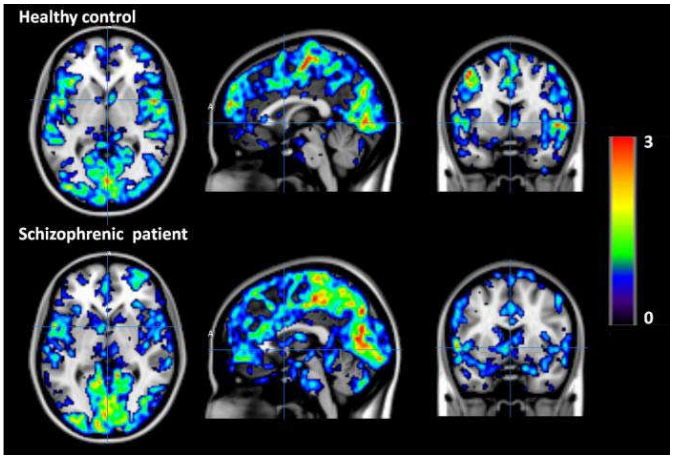

Fig. 9. fMRI DC values of healthy control (top row) and schizophrenic patient (bottom row) during first rs measurement. The DC values are overlaid on the MNI template.

The results presented here are from one healthy and one schizophrenic subject and are only shown to illustrate the potential of measuring and extracting various measures from simultaneously recorded PET, fMRI, and EEG. These measures may then potentially be used as biomarkers for diagnosis and treatment monitoring of schizophrenic patients.

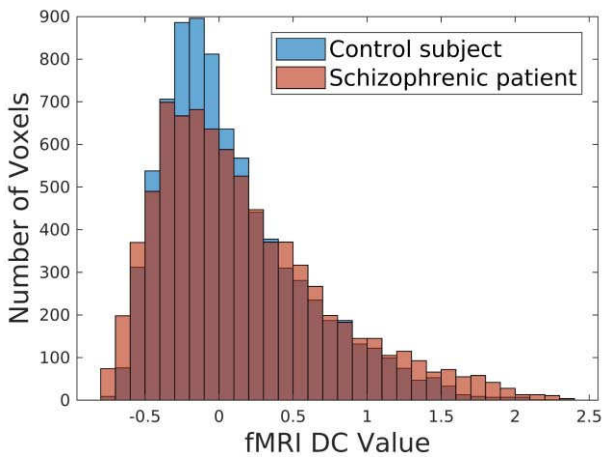

Fig. 10. Histogram plot of the fMRI DC values of the healthy control and the schizophrenic patient in the DMN region.

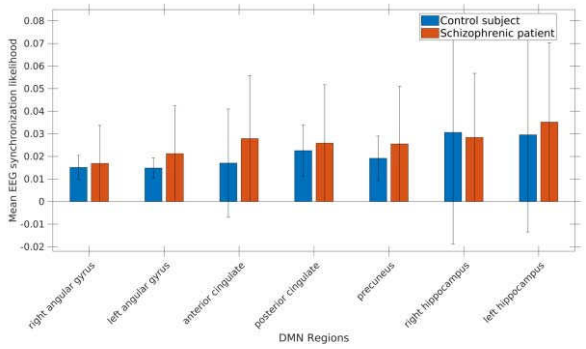

Fig. 11. EEG synchronization likelihood in the DMN regions of the healthy control and the schizophrenic patient.

VI. Discussion and Conclusion

A brief overview with regard to the integration of EEG system to hybrid PET-MR scanners has been presented. Technical challenges, as well as solutions, have also been discussed with critical practical considerations. In addition, the major sources of noise in EEG signals, such as GA, motion, and cardioballistic artifacts, along with possible ways to correct for them, have also been explained above. Practical issues with regard to simultaneous trimodal measurements and considerations for protocol design were discussed with an example of bolus plus infusion protocol in a study with [^{11}C] FMZ. One of the major challenges of multimodal imaging is the data integration. Short overviews about the data integration methods were also discussed. Clinical application was discussed with emphasis on neuro-psychiatry. The simultaneous trimodal study using [^{11}C]ABP688 as the PET tracer, shows the potential of trimodal measurements in schizophrenic patients and the potential use of complementary measures from PET, fMRI, and EEG as biomarkers for diagnosis, treatment planning, and monitoring.

Despite the existence of a great number of technical and practical difficulties in simultaneous trimodal measurements,

the exploratory pilot results presented here show that the complementary information provided by the modalities is very rich. The potential of simultaneous trimodal measurements can be used in various fields of neuroscience, and offer the potential to add value in diagnosis, treatment/surgery planning and the monitoring of disorders.

ACKNOWLEDGMENT

The results presented in this paper are part of the doctoral theses of R. Rajkumar (Dr. rer. medic.), C. Régio Brambilla (Dr. rer. medic.) (Ph.D. DAAD stipend Nr. 57299294), and A. Ruch (Dr. med) and of the Master's thesis of S. Ramkiran (M.Sc. Biomedical Engineering) at the Medical Faculty of the RWTH Aachen University, Germany. The trimodal imaging approach was supported by the EU-FP7 funded project TRIMAGE (Nr. 602621), by the EMDO (Nr. 784) Stiftung to W. Kawohl and by the SFN grant (Nr. P1ZHP3_148704 and PBZHP3_143640) to C. Wyss. The authors would like to thank C. Rick and J. Lewis Bierbrier for proofreading this paper. They would also like to thank A. Muren, C. Frey, S. Frensch, and S. Schaden for their technical assistance and also would like to thank all patients and healthy volunteers for the participation in their trimodal study protocols.

REFERENCES

[1] N. J. Shah *et al.*, "Advances in multimodal neuroimaging: Hybrid MR-PET and MR-PET-EEG at 3 T and 9.4 T," *J. Magn. Reson.*, vol. 229, pp. 101–115, Apr. 2013.

[2] H. F. Wehrl *et al.*, "Simultaneous PET-MRI reveals brain function in activated and resting state on metabolic, hemodynamic and multiple temporal scales," *Nat. Med.*, vol. 19, no. 9, pp. 1184–1189, 2013.

[3] V. Riedl *et al.*, "Local activity determines functional connectivity in the resting human brain: A simultaneous FDG-PET/fMRI study," *J. Neurosci.*, vol. 34, no. 18, pp. 6260–6266, 2014.

[4] H. Herzog, "PET/MRI: Challenges, solutions and perspectives," *Zeitschrift Für Medizinische Physik*, vol. 22, no. 4, pp. 281–298, 2012.

[5] C. Weirich *et al.*, "Analysis and correction of count rate reduction during simultaneous MR-PET measurements with the BrainPET scanner," *IEEE Trans. Med. Imag.*, vol. 31, no. 7, pp. 1372–1380, Jul. 2012.

[6] N. J. Shah *et al.*, "Effects of magnetic fields of up to 9.4 T on resolution and contrast of PET images as measured with an MR-BrainPET," *PLoS ONE*, vol. 9, no. 4, 2014, Art. no. e95250.

[7] L. Tellmann, H. H. Quick, A. Bockisch, H. Herzog, and T. Beyer, "The effect of MR surface coils on PET quantification in whole-body PET/MR: Results from a pseudo-PET/MR phantom study," *Med. Phys.*, vol. 38, no. 5, pp. 2795–2805, 2011.

[8] H.-P. W. Schlemmer *et al.*, "Simultaneous MR/PET imaging of the human brain: Feasibility study," *Radiology*, vol. 248, no. 3, pp. 1028–1035, 2008.

[9] H. Herzog *et al.*, "High resolution BrainPET combined with simultaneous MRI," *Nuklearmedizin*, vol. 50, no. 2, pp. 74–82, 2011

[10] S. Assecondi, C. Lavallee, P. Ferrari, and J. Jovicich, "Length matters: Improved high field EEG-fMRI recordings using shorter EEG cables," *J. Neurosci. Methods*, vol. 269, pp. 74–87, Aug. 2016.

[11] H. B. Hawsawi, D. W. Carmichael, and L. Lemieux, "Safety of simultaneous scalp or intracranial EEG during MRI: A review," *Front. Phys.*, vol. 5, p. 42, Oct. 2017.

[12] P. J. Allen, O. Josephs, and R. Turner, "A method for removing imaging artifact from continuous EEG recorded during functional MRI," *Neuroimage*, vol. 12, no. 2, pp. 230–239, 2000.

[13] V. Krishnaveni, S. Jayaraman, S. Aravind, V. Hariharasudhan, and K. Ramadoss, "Automatic identification and removal of ocular artifacts from EEG using wavelet transform," *Meas. Sci. Rev.*, vol. 6, no. 4, pp. 45–57, 2006.

[14] R. J. Croft and R. J. Barry, "Removal of ocular artifact from the EEG: A review," *Neurophysiologie Clinique*, vol. 50, no. 1, pp. 5–19, 2000.

[15] G. Gratton, M. G. H. Coles, and E. Donchin, "A new method for off-line removal of ocular artifact," *Electroencephalography Clin. Neurophysiol.*, vol. 55, no. 4, pp. 468–484, 1983.

[16] T. Nierhaus *et al.*, "Internal ventilation system of MR scanners induces specific EEG artifact during simultaneous EEG-fMRI," *Neuroimage*, vol. 74, pp. 70–76, Jul. 2013.

[17] S. Rothlubbers, V. Relvas, A. Leal, and P. Figueiredo, "Reduction of EEG artefacts induced by vibration in the MR-environment," in *Proc. Annu. Int. Conf. IEEE Eng. Med. Biol. Soc. (EMBS)*, 2013, pp. 2092–2095.

[18] M. Uji, R. Wilson, S. T. Francis, K. J. Mullinger, and S. D. Mayhew, "Exploring the advantages of multiband fMRI with simultaneous EEG to investigate coupling between gamma frequency neural activity and the BOLD response in humans," *Human Brain Map.*, vol. 39, no. 4, pp. 1673–1687, 2018.

[19] M. E. H. Chowdhury, K. J. Mullinger, P. Glover, and R. Bowtell, "Reference layer artefact subtraction (RLAS): A novel method of minimizing EEG artefacts during simultaneous fMRI," *Neuroimage*, vol. 84, pp. 307–319, Jan. 2014.

[20] J. N. van der Meer *et al.*, "Carbon-wire loop based artifact correction outperforms post-processing EEG/fMRI corrections—A validation of a real-time simultaneous EEG/fMRI correction method," *Neuroimage*, vol. 125, pp. 880–894, Jan. 2016.

[21] J. Jorge, F. Grouiller, R. Gruetter, W. van der Zwaag, and P. Figueiredo, "Towards high-quality simultaneous EEG-fMRI at 7 T: Detection and reduction of EEG artifacts due to head motion," *Neuroimage*, vol. 120, pp. 143–153, Oct. 2015.

[22] G. S. Spencer, J. A. Smith, M. E. H. Chowdhury, R. Bowtell, and K. J. Mullinger, "Exploring the origins of EEG motion artefacts during simultaneous fMRI acquisition: Implications for motion artefact correction," *Neuroimage*, vol. 173, pp. 188–198, Jun. 2018.

[23] G. Bonmassar *et al.*, "Motion and ballistocardiogram artifact removal for interleaved recording of EEG and EPs during MRI," *Neuroimage*, vol. 16, no. 4, pp. 1127–1141, 2002.

[24] P. J. Allen, G. Polizzi, K. Krakow, D. R. Fish, and L. Lemieux, "Identification of EEG events in the MR scanner: The problem of pulse artifact and a method for its subtraction," *Neuroimage*, vol. 8, no. 3, pp. 229–239, 1998.

[25] R. K. Niazy, C. F. Beckmann, G. D. Iannetti, J. M. Brady, and S. M. Smith, "Removal of FMRI environment artifacts from EEG data using optimal basis sets," *NeuroImage*, vol. 28, no. 3, pp. 720–737, 2005.

[26] J. Dammers *et al.*, "Integration of amplitude and phase statistics for complete artifact removal in independent components of neuromagnetic recordings," *IEEE Trans. Biomed. Eng.*, vol. 55, no. 10, pp. 2353–2362, Oct. 2008.

[27] E. Maggioni *et al.*, "Removal of pulse artefact from EEG data recorded in MR environment at 3T. Setting of ICA parameters for marking artefactual components: Application to resting-state data," *PLoS ONE*, vol. 9, no. 11, 2014, Art. no. e112147.

[28] E. R. Kops, H. Hautzel, H. Herzog, G. Antoch, and N. J. Shah, "Comparison of template-based versus CT-based attenuation correction for hybrid MR/PET scanners," *IEEE Trans. Nucl. Sci.*, vol. 62, no. 5, pp. 2115–2121, Oct. 2015.

[29] A. M. Grant *et al.*, "NEMA NU 2-2012 performance studies for the SiPM-based ToF-PET component of the GE SIGNA PET/MR system," *Med. Phys.*, vol. 43, no. 5, p. 2334, 2016.

[30] G. Delso *et al.*, "Performance measurements of the siemens mMR integrated whole-body PET/MR scanner," *J. Nucl. Med.*, vol. 52, no. 12, pp. 1914–1922, Dec. 2011.

[31] R. E. Carson *et al.*, "Comparison of bolus and infusion methods for receptor quantitation: Application to [^{18}F]cyclofoxy and positron emission tomography," *J. Cerebral Blood Flow Metab.*, vol. 13, no. 1, pp. 24–42, 1993.

[32] I. Neuner *et al.*, "Simultaneous trimodal imaging approach using [^{11}C]—Flumazenil for MR-PET-EEG: Feasibility of set-up," presented at the PSMR, Cologne, Germany, May 2016. [Online]. Available: http://psmr.hut-gmbh.net/session/session-6-emerging-applications

[33] T. J. Marczynski, "GABAergic deafferentation hypothesis of brain aging and Alzheimer's disease revisited," *Brain Res. Bull.*, vol. 45, no. 4, pp. 341–379, 1998.

[34] L. Feng *et al.*, "Design of infusion schemes for neuroreceptor imaging: Application to [^{11}C]Flumazenil-PET steady-state study," *BioMed Res. Int.*, vol. 2016, Mar. 2016, Art. no. 9132840. [Online]. Available: https://www.hindawi.com/journals/bmri/2016/9132840/

[35] I. Odano *et al.*, "[^{18}F]Flumazenil binding to central benzodiazepine receptor studies by PET: Quantitative analysis and comparisons with [^{11}C]flumazenil," *Neuroimage*, vol. 45, no. 3, pp. 891–902, 2009.

[36] K. Vanderperren *et al.*, "Removal of BCG artifacts from EEG recordings inside the MR scanner: A comparison of methodological and validation-related aspects," *Neuroimage*, vol. 50, no. 3, pp. 920–934, 2010.

[37] Y. LeCun *et al.*, "Handwritten digit recognition with a back-propagation network," in *Advances in Neural Information Processing Systems 2*. San Mateo, CA, USA: Morgan Kaufmann, 1990, pp. 396–404.

[38] S. M. Plis *et al.*, "Deep learning for neuroimaging: A validation study," *Front. Neurosci*, vol. 8, no. 8, p. 229, 2014.

[39] R. Polikar, C. Tilley, B. Hillis, and C. M. Clark, "Multimodal EEG, MRI and PET data fusion for Alzheimer's disease diagnosis," in *Proc. IEEE 32nd Annu. Int. Conf. Eng. Med. Biol. Soc.*, Aug./Sep. 2010, pp. 6058–6061.

[40] F. Biessmann, S. Plis, F. C. Meinecke, T. Eichele, and K. R. Müller, "Analysis of multimodal neuroimaging data," *IEEE Rev. Biomed. Eng.*, vol. 4, pp. 26–58, Oct. 2011. [Online]. Available: https://ieeexplore.ieee.org/document/6035960

[41] S. Dähne *et al.*, "Multivariate machine learning methods for fusing multimodal functional neuroimaging data," *Proc. IEEE*, vol. 103, no. 9, pp. 1507–1530, Sep. 2015.

[42] I. Neuner *et al.*, "Multimodal imaging utilising integrated MR-PET for human brain tumour assessment," *Eur. Radiol.*, vol. 22, no. 12, pp. 2568–2580, 2012.

[43] J. Sui, T. Adali, Q. Yu, J. Chen, and V. D. Calhoun, "A review of multivariate methods for multimodal fusion of brain imaging data," *J. Neurosci. Methods*, vol. 204, no. 1, pp. 68–81, 2012.

[44] J. Daunizeau, H. Laufs, and K. J. Friston, *EEG-fMRI Information Fusion: Biophysics and Data Analysis*. Heidelberg, Germany: Springer, 2010, ch. 25. [Online]. Available: https://link.springer.com/book/10.1007/978-3-540-87919-0#about

[45] R. J. Huster, S. Debener, T. Eichele, and C. S. Herrmann, "Methods for simultaneous EEG-fMRI: An introductory review," *J. Neurosci.*, vol. 32, no. 18, pp. 6053–6060, 2012.

[46] H. Hampel *et al.*, "In vivo imaging of region and cell type specific neocortical neurodegeneration in Alzheimer's disease: Perspectives of MRI derived corpus callosum measurement for mapping disease progression and effects of therapy. Evidence from studies with MRI, EEG and PET," *J. Neural Transm.*, vol. 109, nos. 5–6, pp. 837–855, 2002.

[47] K. Uludağ and A. Roebroeck, "General overview on the merits of multimodal neuroimaging data fusion," *Neuroimage*, vol. 102, pp. 3–10, Nov. 2014.

[48] S. Liu *et al.*, "Multimodal neuroimaging computing: A review of the applications in neuropsychiatric disorders," *Brain Informat.*, vol. 2, no. 3, pp. 167–180, 2015.

[49] R. O'Halloran, B. H. Kopell, E. Sprooten, W. K. Goodman, and S. Frangou, "Multimodal neuroimaging-informed clinical applications in neuropsychiatric disorders," *Front. Psychiatry*, vol. 7, p. 63, Apr. 2016.

[50] M. Laruelle *et al.*, "Microdialysis and SPECT measurements of amphetamine-induced dopamine release in nonhuman primates," *Synapse*, vol. 25, no. 1, pp. 1–14, 1997.

[51] N. J. Shah *et al.*, "Multimodal fingerprints of resting state networks as assessed by simultaneous trimodal MR-PET-EEG imaging," *Sci. Rep.*, vol. 7, no. 1, p. 6452, 2017.

[52] A. Del Guerra *et al.*, "TRIMAGE: A dedicated trimodality (PET/MR/EEG) imaging tool for schizophrenia," *Eur. Psychiatry*, vol. 50, pp. 7–20, Apr. 2017.

[53] W. P. Spooren *et al.*, "Anxiolytic-like effects of the prototypical metabotropic glutamate receptor 5 antagonist 2-methyl-6-(phenylethynyl)pyridine in rodents," *J. Pharmacol. Exp. Ther.*, vol. 295, no. 3, pp. 1267–1275, 2000.

[54] W. P. J. M. Spooren, F. Gasparini, T. E. Salt, and R. Kuhn, "Novel allosteric antagonists shed light on mGlu$_5$ receptors and CNS disorders," *Trends Pharmacol. Sci.*, vol. 22, no. 7, pp. 331–337, 2001.

[55] E. Tatarczyñska *et al.*, "Potential anxiolytic-and antidepressant-like effects of MPEP, a potent, selective and systemically active mGlu5 receptor antagonist," *Brit. J. Pharmacol.*, vol. 132, no. 7, pp. 1423–1430, 2001.

[56] T. Ohnuma, S. J. Augood, H. Arai, P. J. McKenna, and P. C. Emson, "Expression of the human excitatory amino acid transporter 2 and metabotropic glutamate receptors 3 and 5 in the prefrontal cortex from normal individuals and patients with schizophrenia," *Brain Res. Mol. Brain Res.*, vol. 56, nos. 1–2, pp. 207–217, 1998.

[57] D. Martinez *et al.*, "Imaging glutamate homeostasis in cocaine addiction with the metabotropic glutamate receptor 5 positron emission tomography radiotracer [^{11}C]ABP688 and magnetic resonance spectroscopy," *Biol. Psychiatry*, vol. 75, no. 2, pp. 165–171, 2014.

[58] D. Elmenhorst *et al.*, "Circadian variation of metabotropic glutamate receptor 5 availability in the rat brain," *J. Sleep Res.*, vol. 25, no. 6, pp. 754–761, 2016.

[59] S. M. Ametamey *et al.*, "Human PET studies of metabotropic glutamate receptor subtype 5 with 11C-ABP688," *J. Nucl. Med.*, vol. 48, no. 2, pp. 247–252, 2007.

[60] C. R. Brambilla *et al.*, "Bolus infusion scheme for C-11-ABP688 in multimodal studies with PET/MR/EEG," presented at the Jahrestagung Der Deutschen Gesellschaft Für Nuklearmedizin, Bremen, Germany, 2018. [Online]. Available: http://psmr.hut-gmbh.net/session/session-6-emerging-applications

[61] C. Burger *et al.*, "Evaluation of a bolus/infusion protocol for 11C-ABP688, a PET tracer for mGluR5," *Nucl. Med. Biol.*, vol. 37, no. 7, pp. 845–851, 2010.

[62] E. R. Kops and H. Herzog, "Template based attenuation correction for PET in MR-PET scanners," in *Proc. IEEE Nucl. Sci. Symp. Conf. Rec.*, Dresden, Germany, 2008, pp. 3786–3789.

[63] V. Treyer *et al.*, "Evaluation of the metabotropic glutamate receptor subtype 5 using PET and 11C-ABP688: Assessment of methods," *J. Nucl. Med. Off. Publ. Soc. Nucl. Med.*, vol. 48, no. 7, pp. 1207–1215, 2007.

[64] C. G. Yan, X.-D. Wang, X. N. Zuo, and Y.-F. Zang, "DPABI: Data processing & analysis for (resting-state) brain imaging," *Neuroinformatics*, vol. 14, no. 3, pp. 339–351, 2016.

[65] R. L. Buckner *et al.*, "Cortical hubs revealed by intrinsic functional connectivity: Mapping, assessment of stability, and relation to Alzheimer's disease," *J. Neurosci.*, vol. 29, no. 6, pp. 1860–1873, 2009.

[66] W. R. Shirer, S. Ryali, E. Rykhlevskaia, V. Menon, and M. D. Greicius, "Decoding subject-driven cognitive states with whole-brain connectivity patterns," *Cerebral Cortex*, vol. 22, no. 1, pp. 158–165, 2012.

[67] S. M. Smith *et al.*, "Advances in functional and structural MR image analysis and implementation as FSL," *Neuroimage*, vol. 23, no. S1, pp. 208–219, 2004.

[68] C. J. Stam and B. W. Van Dijk, "Synchronization likelihood: An unbiased measure of generalized synchronization in multivariate data sets," *Physica D Nonlin. Phenomena*, vol. 163, nos. 3–4, pp. 236–251, 2002.

[69] D. S. Bassett and E. Bullmore, "Small-world brain networks," *Neuroscientist*, vol. 12, no. 6, pp. 512–523, Dec. 2006.

[70] A. Delorme and S. Makeig, "EEGLAB: An open source toolbox for analysis of single-trial EEG dynamics including independent component analysis," *J. Neurosci. Methods*, vol. 134, no. 1, pp. 9–21, 2004.

[71] T.-W. W. Lee, M. Girolami, and T. J. Sejnowski, "Independent component analysis using an extended infomax algorithm for mixed subgaussian and supergaussian sources," *Neural Comput.*, vol. 11, no. 2, pp. 417–441, 1999.

[72] M. Chaumon, D. V. M. Bishop, and N. A. Busch, "A practical guide to the selection of independent components of the electroencephalogram for artifact correction," *J. Neurosci. Methods*, vol. 250, pp. 47–63, Jul. 2015.

[73] R. D. Pascual-Marqui, C. M. Michel, and D. Lehmann, "Low resolution electromagnetic tomography: A new method for localizing electrical activity in the brain," *Int. J. Psychophysiol.*, vol. 18, no. 1, pp. 49–65, 1994.